Global stability analysis of the axisymmetric boundary layer: Effect of axisymmetric forebody shapes on the helical global modes

RAMESH BHORANIYA[1] [ID],* and VINOD NARAYANAN[2]

[1]Department of Mechanical Engineering, Marwadi University, Rajkot 360 003, India
[2]Department of Mechanical Engineering, Indian Institute of Technology, Palaj, Gandhinagar 382 355, India
*Corresponding author. E-mail: rameshkumar.bhoraniya@marwadieducation.edu.in

Abstract.   The effects of different axisymmetric forebody shapes have been studied on the non-axisymmetric (helical) global modes of the boundary layer developed on a circular cylinder. Sharp cone, ellipsoid and paraboloid shapes have been considered with the fineness ratio (FR) of 2.5, 5.0 and 7.5. The base flow is in line with the cylinder's axis at the inflow boundary, and hence the base flow is axisymmetric. The boundary layer has developed from the tip of the forebody where a highly favourable pressure gradient exists, and it depends on the sharp edge of the forebody's geometric shape. However, the pressure gradient then remains constant on the cylindrical surface of the main body. Thus, the boundary layer developed on the forebody and main body (cylinder) is non-parallel, non-similar and axisymmetric. The governing equations for the stability analysis of the small disturbances have been derived in the cylindrical polar coordinates. The spectral collocation method with Chebyshev polynomials has been used to discretise the stability equations. An eigenvalue problem has been formulated from the discretised stability equations along with the appropriate boundary conditions. The numerical solution of the eigenvalue problem was done using Arnoldi's iterative algorithm. The global temporal modes have been computed for helical modes $N = 1$, 2, 3, 4 and 5 for Reynolds number $Re = 2000$, 4000 and 10000. The spatial and temporal structures of the least stable global modes have been studied for different Reynolds numbers and helical modes. The global modes with ellipsoid were found the least stable while that of the sharp cone were found the most stable.

Keywords.   Forebody; global stability; axisymmetric; boundary layer; helical modes.

PACS Nos   47.20.Ft; 47.20.Ib; 47.20.k

1. Introduction

When viscous fluid flows over a sharp axisymmetric body, a boundary layer develops in the flow direction from the body's tip (leading edge) and grows continuously along the direction of the stream. The boundary layer is always laminar near the leading edge due to the very small thickness of the boundary layer. The boundary layer thickness gradually increases in the streamwise direction, and thus Reynolds number also. At a particular streamwise location, the Reynolds number exceeds the critical values, and flow becomes unstable, leading to the growth of small disturbances and transition of laminar flow to turbulence. Under the effect of the strongly favourable pressure gradient in the flow direction, the flow becomes accelerating, and boundary layer growth reduces, which reduces the Reynolds number and helps keep the boundary layer laminar. However,

the boundary layer thickness is strongly affected by the Reynolds number rather than pressure gradients. Sometimes, even with a favourable pressure gradient at a high Reynolds number, a transition occurs. The forebody attached to the main body (cylinder) generates a favourable pressure gradient, which remains unchanged on the cylindrical surface. Thus, the stability analysis helps delay the boundary layer's transition and maximise the laminar regime of the boundary layer, which finally reduces the drag forces acting on the axisymmetric propulsive bodies [1].

Vinod and Govindarajan [2] studied the relation between instabilities and birth of the turbulent spot using numerical solution of eigenvalue problem and found that standard results for Tollmien–Schlichting (T-S) route is followed at low noise level and a by-pass route is followed at higher noise level. In both the routes, the birth of the turbulent spot depends on the pattern of secondary

instabilities. Casarella *et al* [3] found that a sharper body generates a more favourable pressure gradient and a blunt body generates less favourable gradients. Parsons and Goodson [1] studied and concluded that the intention of the delaying transition is to maximise the laminar regime in the boundary layer and thus to reduce the viscous drag on the axisymmetric-type propulsive bodies like submarines, torpedoes, missiles and rockets. Aerodynamic stability is essential for guided aerodynamic vehicles like missiles to control their trajectories for the targets. It has been found that natural axisymmetric laminar bodies have a minimum drag and allows a long run of laminar flow. It is expected to have a minimum drag for energy efficiency in the design of vehicles like fuselages, missiles, torpedoes and submarines. Recently, James *et al* [4] and Holmes *et al* [5] found that when the pressure gradient is favourable on the smooth surface of the airplane, long run of the laminar boundary layer can be achieved which reduces a significant amount of drag. Carmichael [6] has conducted experiments on NACA-66 airfoil about its longitudinal axis with a low fineness ratio (FR). They found that low FR and appropriate shape generate a robust favourable pressure gradient on the axisymmetric body, which helps to keep the boundary layer in the laminar regime over a more substantial length of the body. Many researchers studied the characteristics of the base flow field around the shape of the body of revolutions with full applications in aerodynamics and marine hydrodynamics. They found that sharp-edged bodies with hyperbolic and parabolic nose experience less drag than spherical and elliptical shapes.

Theofilis [7], Alizard and Robinet [8] and Akervik *et al* [9] have studied temporal and spatial instabilities of the flat-plate boundary layer, and global modes have been found stable in all these cases. Thus, the stability analysis helps in delaying the transition of the boundary layer and maximising the laminar regime of the boundary layer, which finally reduces the drag forces acting on the axisymmetric propulsive bodies [1]. In the local stability analysis of Rao [10], Tutty and Price [11] and Vinod and Govindarajan [2] of the axisymmetric boundary layer on a circular cylinder, they assumed that the boundary layer develops directly on the surface of the cylinder only. However, the main body of the submarines, torpedoes and missiles are equipped with specific geometry at the leading edge. This specific portion of the body is known as the forebody. In the present study, the authors have considered sharp cone, paraboloid and ellipsoid with FR = 2.5, 5.0 and 7.5 to study their effect on global stability characteristics. The intensity of the favourable pressure gradient depends on the sharpness or bluntness of the fore-body shape. Sharp cone and paraboloid are sharper than ellipsoid, and smaller FR gives more sharpness to the forebody.
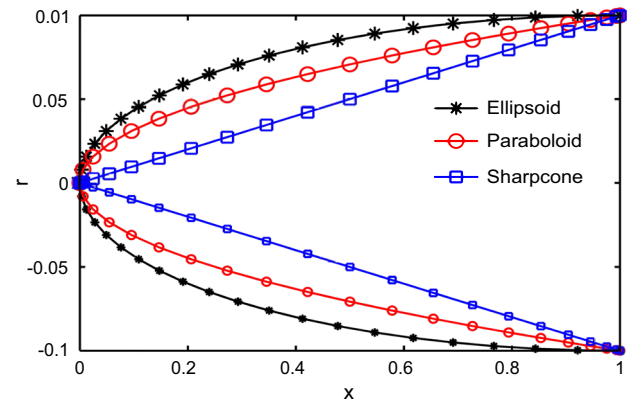
Figure 1. Schematic diagram of different axisymmetric forebody shapes (*eaf* section as shown in figure 2) with FR = 5.0. FR is the length to diameter ratio (L/D) of different forebody shapes.
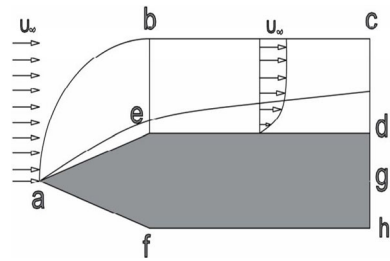
Figure 2. Schematic diagram of axisymmetric boundary layer on a circular cylinder with axisymmetric forebody. The axisymmetric domain *bcde* is used for the global instability analysis. Domain *aeb* is included in the base flow computation.

The geometry of the three forebody shapes with FR = 5.0 is shown in figure 1.

The global stability analysis of the axisymmetric boundary layer on a circular cylinder was performed by Bhoraniya and Narayanan [12,13]. They found that increased semi-cone angle increases the intensity of the favourable pressure gradient and stabilises the boundary layer. Bhoraniya and Narayanan [14] also studied the comparison of the axisymmetric boundary layer's global modes on a circular cylinder with the hemispherical cap with a blunt cylinder. Bhoraniya and Narayanan [15] studied the effect of different forebody shapes on the axisymmetric modes with different FR. They found global modes the least stable for ellipsoid geometry and the most stable for sharp cone for a given Reynolds number and FR. Similarly, for a smaller FR, global modes are found the most stable, and for a larger FR, global modes are the least stable.

In boundary layer flows, a pure convectively unstable open system is involved, and some form of steady periodic forcing is present such as free stream turbulence coupling with disturbance waves at the solid trailing

edge. Gaster [19], Michalke [20], Tam [21] and many others have studied such downstream evolution of the linear disturbances in a long time limit using spatial stability theory. Chomaz *et al* [22,23], Pierrehumbert [24], Koch [25] in their investigations found that the existence of a region of local absolute instability was a necessary but not a sufficient condition. Monkewitz *et al* [26] showed a sequence of transition in the cylinder wake with increased Reynolds number; first, the transition from stability to convective instability, then from convective to local absolute instability and finally the bifurcation to a self-sustained global mode only after a sufficiently large portion of the flow has become absolutely unstable.

Open flows such as mixing layers, jet, separation bubbles and boundary layers develop extended domain in which fluid particles are continuously advected downstream and behave either as a noise amplifier or as oscillators, both of which have strong non-linearities [27]. The widely separated scale does not characterise the length scale for basic flow and disturbances in a fully global context. Then, the flow dynamics are viewed as the interaction of the all-global modes in the physical domain in the streamwise direction. The noise amplifier behaviour of the boundary layer emphasises strongly on the peculiar non-orthogonality of linear global modes. The linear evolution operator governing the global modes exhibits a peculiar non-normality due to the basic advection. It is now well established that, as a result of non-normality, the perturbation energy may experience a transient growth for a small period of time, even for decaying eigenmodes.

Authors have already studied the effect of three different forebody shapes, sharp cone, paraboloid and ellipsoid, on the axisymmetric global modes [15] and the present work is the extension of the previous work. The main objective of the present paper is to study the effect of different forebody shapes on the non-axisymmetric (helical) global modes of the axisymmetric boundary layer. The global modes have been analysed for these three forebody shapes for different Reynolds numbers, azimuthal wave number and FR. The governing equations of the perturbations are linearised and modal stability analysis has been performed for the axisymmetric boundary layer.

2. Problem formulation

A circular cylinder of finite length and body radius of a has been considered in the uniform stream of incompressible fluid. Sharp cone, paraboloid and ellipsoid forebody shapes have been considered with FR = 2.5, 5.0 and 7.5. The boundary layer developed on such a

cylinder is two-dimensional and the favourable pressure gradient developed in the streamwise direction depends on the geometric shape and FR value of the forebody. The Reynolds number (Re) is computed based on the body radius of the cylinder.

$$Re = \frac{U_\infty a}{\nu}, \tag{1}$$

where a is the body radius of the cylinder, U_∞ is the free-stream velocity and ν is the kinematic viscosity.

The governing stability equations have been derived in the cylindrical coordinates (r, θ, z) from the Navier–Stokes equations of the base flow. The base flow is axisymmetric and disturbances are three-dimensional. The instantaneous flow quantities are split into the base and perturbed flow quantities.

$$\overline{U} = U + u, \quad \overline{V} = V + v,$$
$$\overline{W} = 0 + w, \quad \overline{P} = P + p, \tag{2}$$

where u, v and w are the velocity perturbations in the axial, radial and azimuthal directions respectively and p is the pressure perturbations. U and V are base velocity components in the axial and radial directions and P is the basic pressure. $\overline{U}, \overline{V}, \overline{W}$ are the instantaneous velocity components in the axial, radial and azimuthal directions and $\overline{P}$ is the instantaneous pressure. The normal mode form of the disturbances were considered and they are varying in the two non-homogeneous directions, axial and radial, respectively.

$$\mathbf{q}(x, r, \theta, t) = \hat{\mathbf{q}}(x, r)e^{[i(N\theta - \omega t)]}, \tag{3}$$

where $\mathbf{q} = [u, v, w, p]$, $\mathbf{Q} = [U, V, P]$, $\overline{\mathbf{Q}} = [\overline{U}, \overline{V}, \overline{P}]$, where q, Q, $\overline{Q}$, N and ω are perturbations, base flow quantities, instantaneous flow quantities, azimuthal wave number and complex circular frequency respectively. The governing stability equations for the global stability analysis are as follows:

$$\frac{\partial u}{\partial t} + U\frac{\partial u}{\partial x} + u\frac{\partial U}{\partial x} + V\frac{\partial u}{\partial r} + v\frac{\partial U}{\partial r} + \frac{\partial p}{\partial x}$$
$$- \frac{1}{Re}[\nabla^2 u] = 0, \tag{4}$$

$$\frac{\partial v}{\partial t} + U\frac{\partial v}{\partial x} + u\frac{\partial V}{\partial x} + V\frac{\partial v}{\partial r} + v\frac{\partial V}{\partial r} + \frac{\partial p}{\partial r}$$
$$- \frac{1}{Re}\left[\nabla^2 v - \frac{v}{r^2} - \frac{2}{r^2}\frac{\partial w}{\partial \theta}\right] = 0, \tag{5}$$

$$\frac{\partial w}{\partial t} + U\frac{\partial w}{\partial x} + V\frac{\partial w}{\partial r} + V\frac{w}{r} + \frac{1}{r}\frac{\partial p}{\partial \theta}$$
$$- \frac{1}{Re}\left[\nabla^2 w - \frac{w}{r^2} + \frac{2}{r^2}\frac{\partial v}{\partial \theta}\right] = 0, \tag{6}$$

$$\frac{\partial u}{\partial x} + \frac{\partial v}{\partial r} + \frac{v}{r} + \frac{1}{r}\frac{\partial w}{\partial \theta} = 0, \tag{7}$$

where

$$\nabla^2 = \frac{\partial^2}{\partial x^2} + \frac{\partial^2}{\partial r^2} + \frac{1}{r}\frac{\partial}{\partial r} + \frac{1}{r^2}\frac{\partial^2}{\partial\theta^2} = 0. \tag{8}$$

2.1 *Boundary conditions*

On the cylinder wall, due to viscous effect and non-porous wall, the tangential, radial and azimuthal disturbance velocity components are zero.

$$u(x, a) = 0, \; v(x, a) = 0, \; w(x, a) = 0. \tag{9}$$

The velocity and pressure disturbances are expected to reduce gradually in the radial direction away from the solid wall of the cylinder and approaches zero at distances far away from the wall.

$$u(x, \infty) = 0, \; v(x, \infty) = 0,$$
$$p(x, \infty) = 0, \; w(x, \infty) = 0. \tag{10}$$

As already explained in [15], global stability solution needs boundary conditions along the streamwise direction at the inflow and outflow boundaries. Homogeneous Dirichlet boundary conditions (eq. (11)) at the inflow boundary and linear extrapolation-type boundary conditions (eq. (14)) at the outflow boundary are applied on the velocity disturbances for numerically solving the eigenvalue problem [7–9,16–18].

$$u(x_{in}, r) = 0, \; v(x_{in}, r) = 0, \; w(x_{in}, r) = 0 \tag{11}$$
$$u_{n-2}[x_n - x_{n-1}] - u_{n-1}[x_n - x_{n-2}]$$
$$+ u_n[x_{n-1} - x_{n-2}] = 0 \tag{12}$$
$$v_{n-2}[x_n - x_{n-1}] - v_{n-1}[x_n - x_{n-2}]$$
$$+ v_n[x_{n-1} - x_{n-2}] = 0 \tag{13}$$
$$w_{n-2}[x_n - x_{n-1}] - w_{n-1}[x_n - x_{n-2}]$$
$$+ w_n[x_{n-1} - x_{n-2}] = 0. \tag{14}$$

At the wall, physically no boundary condition exists for the pressure. In the incompressible flow instability computations, pressure compatibility conditions have been applied successfully [7,28–30]. Considering no-slip conditions at the cylinder wall, the pressure compatibility conditions for the cylindrical coordinates reduces as

$$\frac{\partial p}{\partial x} = \frac{1}{Re}\left[\frac{\partial^2 u}{\partial r^2} + \frac{1}{r}\frac{\partial u}{\partial r}\right] \tag{15}$$

$$\frac{\partial p}{\partial r} = \frac{1}{Re}\left[\frac{\partial^2 v}{\partial r^2} + \frac{1}{r}\frac{\partial v}{\partial r}\right]. \tag{16}$$

The linearised pressure Poisson's equation (LPPE) has been implemented instead of pressure compatibility conditions to avoid the non-physical solution of the two- and three-dimensional eigenvalue problems [31]. Bhoraniya and Narayanan [14] have shown that the spectra

obtained using compatibility conditions and LPPE have an excellent agreement with the appropriate use of sponge region near the outflow boundary [14].

2.2 *Discretisation of stability equations and solution*

A spectral collocation with Chebyshev polynomials has been used to discretise the primitive form of the governing stability equations. In the present form of the stability equations, first and second derivatives of the disturbance velocities u, v and w are involved. Because of the global nature of the discretisation scheme, the accuracy of the spectral collocation is superior to all other discretisation methods. However, due to the global nature, it includes all the collocation points within the domain for computation at any grid point and thus it is a full matrix method. Thus, a demanding computational facility is required for the numerical solution of global stability problems. The first and second derivatives of the disturbance quantities are less sensitive to discretisation error, and one can expect a better accuracy at the moderate spatial resolution.

$$x_c = \cos\left(\frac{\pi i}{n}\right) \quad \text{for} \quad i = 0, 1, 2, 3, \ldots, n \tag{17}$$
$$x_{\text{real}} = (1 - x_c)L_x/2 + x_{\text{min}} \tag{18}$$
$$r_c = \cos\left(\frac{\pi j}{m}\right) \quad \text{for} \quad j = 0, 1, 2, 3, \ldots, m. \tag{19}$$

In the near wall region, stretching of the collocation points has been implemented to improve spatial resolution. Equation (20) given by [32] has been used to capture the physics of disturbances.

$$r_{\text{real}} = \frac{r_i L_r (1 - r_c)}{L_r + r_c(L_r - 2r_i)} + a. \tag{20}$$

A general eigenvalue problem has been formulated as follows:

$$\begin{bmatrix} A_{11} & A_{12} & A_{13} & A_{14} \\ A_{21} & A_{22} & A_{23} & A_{24} \\ A_{31} & A_{32} & A_{33} & A_{34} \\ A_{41} & A_{42} & A_{43} & A_{44} \end{bmatrix} \begin{bmatrix} u_r \\ u_\theta \\ u_\phi \\ p \end{bmatrix}$$
$$= i\omega \begin{bmatrix} B_{11} & B_{12} & B_{13} & B_{14} \\ B_{21} & B_{22} & B_{23} & B_{24} \\ B_{31} & B_{32} & B_{33} & B_{34} \\ B_{41} & B_{42} & B_{43} & B_{44} \end{bmatrix} \begin{bmatrix} u_r \\ u_\theta \\ u_\phi \\ p \end{bmatrix}$$
$$[A][\phi] = i\omega[B][\phi], \tag{21}$$

where A and B are square matrices of size $4 \times n \times m$, $i\omega$ is an eigenvalue and ϕ is a vector of unknown amplitude of disturbance flow quantities u, v, w and p.

2.3 *Base flow solution*

The velocity profile of the boundary layer developed on the considered axisymmetric bodies was obtained by numerical solution of the steady N-S equation for the axisymmetric domain. The inflow velocity component is parallel to the axis of the cylinder and therefore base flow is axisymmetric. The finite volume code ANSYS Fluent was used with second-order accurate scheme. The grid convergence test was performed to check the accuracy of the computed base flow. The effect of forebody shape and FR on the base flow profile is already analysed in the previous work of the authors [15]. It has been found that forebody shape and FR significantly modify the base flow and affect transverse curvature, shape factor and non-parallel effects. It affects transverse curvature near the leading edge of the boundary layer. This effect gradually reduces in the streamwise direction towards the downstream. Readers are requested to refer [15] for a detailed discussion on the base-flow solution, the effect of different shapes and FR on the base-flow velocity profile. Thus, the modified base flow significantly affects the stability of the boundary layer.

3. Code validation

The global nature of the problem is reduced to an equivalent of local stability problems for the preliminary comparison of the stability results. The streamwise domain length of one wavelength ($L_x = 2\pi/\alpha$) is considered for the least stable helical mode, $N = 1$. The base-flow velocity profile considered is the same at all the streamwise locations to remove non-parallel effects. i.e. $V = 0$ and $(\partial U/\partial x) = 0$. In the wall-normal direction, the boundary conditions are the same as that of local stability analysis [7]. In the streamwise direction at the inlet and the outlet, Robin and periodic conditions are applied to impose wave-like behaviour of the disturbances [17]. The Robin conditions with the constant streamwise wave number (α) prescribed at the inlet and the outlet are derived from $\phi(r, t) = \hat{\phi}(r)e^{[i(N\theta - \omega t)]}$.

$$\frac{\partial^2 u}{\partial x^2} = -\alpha^2 u, \quad \frac{\partial^2 v}{\partial x^2} = -\alpha^2 v, \quad \frac{\partial^2 w}{\partial x^2} = -\alpha^2 w \quad (22)$$
$$u(x, r) = u(x + L_x, r), \quad v(x, r) = v(x + L_x, r)$$
$$w(x, r) = w(x + L_x, r). \quad (23)$$

The boundary conditions shown in eq. (22) are applied to the disturbance velocity components in the streamwise direction at the inflow boundary. The second derivatives of velocity disturbances are considered to avoid complex quantities in the boundary conditions,
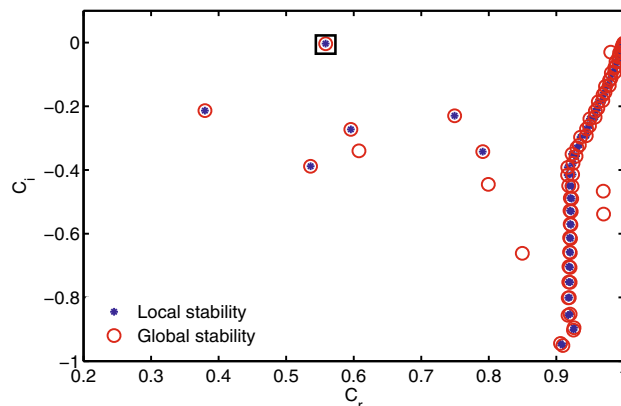

Figure 3. Comparison of the eigenspectrum of global stability analysis with the local stability analysis of Tutty and Price [11] for the helical mode ($N = 1$) and Reynolds number $Re = 1060$. Here $Re = 1060$ is the critical Reynolds number for local stability analysis based on the body radius of the cylinder.

and hence fast computations can take place. The boundary conditions in the radial direction at the cylinder wall and far-field are the same as that of the local stability analysis. The critical Reynolds number, streamwise wave number and streamwise location are 1060, 0.125 and 543 respectively for the helical mode, $N = 1$ [11]. The Reynolds number is computed based on the body radius of the cylinder. The streamwise domain length of one wavelength is equal to $L_x = 0.786$. The streamwise domain size is very small, and hence the convergence of computations took place with 41 and 101 collocation points in the streamwise and wall-normal direction. The comparison of the eigenspectra and eigenfunctions are shown in figures 3 and 4. The eigenspectra of the local and global approaches are in good agreement. The eigenfunctions presented for the least stable eigenmodes for u, v and w velocity disturbances are also in full agreement with each other. The streamwise wave number (α) is also computed from the disturbance amplitudes u, v and w, and it is equal to 0.125. Thus, the approach used for the numerical solution of two-dimensional eigenvalue problem is validated against the available classical results in the open literature.

4. Results and discussions

The global modes of the axisymmetric boundary layer have been computed for three different Reynolds number $Re = 2000$, 5000 and 10000, helical modes $N = 1$, 2, 3, 4 and 5, forebody shapes sharp cone, ellipsoid and paraboloid and FR = 2.5, 5.0 and 7.5. The computational domain sizes of the axial and radial directions are

(a)

(b)

(c)
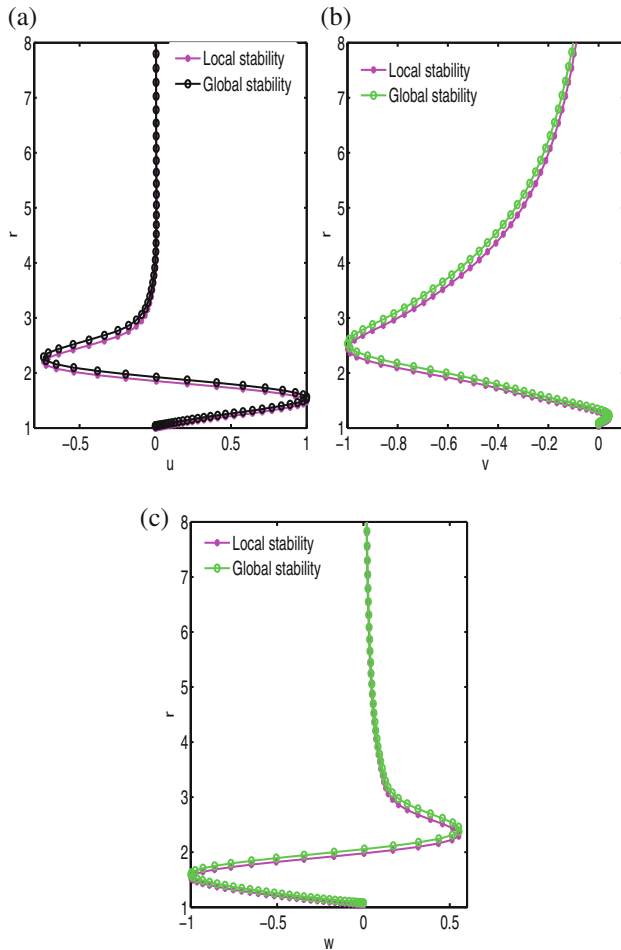
Figure 4. Comparisons of the real parts of (**a**) streamwise u, (**b**) wall normal v and (**c**) azimuthal w eigenfunctions for local and global stability analysis for the helical mode ($N = 1$) for $Re = 1060$ based on the body radius of the cylinder.

considered as $150a$ and $5a$, respectively. The Reynolds number is computed based on the cylinder radius. The number of collocation points considered in the axial and radial directions are 241 and 61, respectively. To prevent spurious reflection of the waves at the outflow boundary, heavy sponging is applied near the outflow boundary. A hyperbolic tangent function has been used to model a sponge region near the downstream in the flow direction. It has been checked that sponging is not affecting the results of the numerical solution of the eigenvalue problem.

4.1 *Grid convergence study*

It is essential to check that the number of collocation points taken to model the flow domain in the axial and radial directions are sufficient for the spatial resolution and thus to get solution independent of the grid size. The test has been performed for a paraboloid shape

with FR $= 5.0$, $N = 1$ and $Re = 2000$. A course grid (Mesh #3) with $n = 171$ collocation points in the axial and $m = 47$ in the radial directions were selected successively refined by a factor of 1.142. Two least stable eigenmodes were computed for three different grid sizes, as reported in table 1. A relative error between two consecutive eigenvalues for the real and imaginary parts was computed, and the largest one is reported in table 1. The grid size #1 has been adopted in all stability results reported in this manuscript.

### 4.2 *Effect of different forebody shapes on global temporal modes*

To study the effect of different axisymmetric forebody shapes on the global modes, the 2D eigenvalue problem was solved for $Re = 2000$ and FR $= 2.5$ with the streamwise domain size of 150. Figure 5a shows the comparison of the discrete part of the eigenspectra for $N = 1$, $Re = 2000$ and FR $= 2.5$ for different forebody shapes. The comparison shows that the eigenmodes with the ellipsoid forebody are the least stable and with the sharp-cone are the most stable. However, the imaginary part of the least stable global modes are negative, and hence the flow is temporally stable. The frequency distribution (ω_r) has almost similar pattern for all three forebody shapes. The temporal growth rate for other helical modes $N = 2, 3, 4$ and 5 is also studied (not presented here), and a similar pattern has been observed. A marginal difference in the temporal growth was observed between the paraboloid and the sharp cone in the case of axisymmetric mode ($N = 0$) [15]. However, in the present study, significant difference in the temporal growth has been observed between the paraboloid and the sharp cone for the helical mode ($N = 1$).

4.3 *Local convective stability analysis*

A convective stability analysis (local stability) was also performed to verify the trends of the global temporal modes of the boundary layer. In the convective stability analysis, streamwise wave number ($\alpha = \alpha_r + \alpha_i$) is complex and circular frequency (ω) is real. We considered a constant ω_r for all the three forebody shapes and computed α_i at different streamwise locations to compare the spatial growth rate of the disturbances. A polynomial eigenvalue problem was formulated and was solved using polyeig function of the MATLAB. A frequency $\omega_r = 0.15$ was selected from the eigenspectra of the global stability analysis (figure 5a) for $Re = 2000$, $N = 1$ and FR $= 2.5$. The spatial growth rate α_i was computed at different streamwise locations. From figure

Table 1. The grid convergence study for two least stable eigenmodes ω_1 and ω_2 for $Re = 2000$, helical mode $N = 1$, parabolic forebody with FR = 2.5, and three different grid sizes. The grid refinement ratio of 1.142 is used to improve the resolution in the axial and radial directions. The maximum absolute error (ϵ) is shown here.

Mesh	L_x	L_r	$n \times m$	n	m	ω_1	ω_2	ϵ (%)
#1	150	5	13481	221	61	0.03757–0.01393i	0.04245–0.0140i	2.17
#2	150	5	10229	193	53	0.03713–0.01364i	0.04195–0.01346i	4.09
#3	150	5	8037	171	47	0.03685–0.01282i	0.04161–0.01293i	–
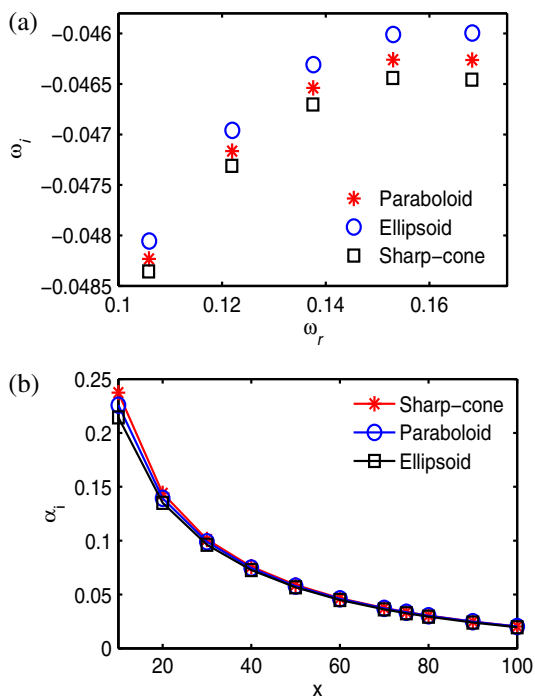
Figure 5. (**a**) Comparison of the eigenspectra for $N = 1$, $Re = 2000$ and FR = 2.5, (**b**) comparison of the spatial growth rate (α_i) at different streamwise locations for $N = 1$, $Re = 2000$, FR = 2.5 and $\omega_r = 0.15$.

Figure 6. Comparison of the spatial eigenmodes at streamwise location $x = 75$ for $N = 1$, $Re = 2000$ and FR = 2.5. The frequency of all the least stable eigenmodes are nearer to $\omega = 0.15$.

5b, we can see that the spatial growth rate in the streamwise direction and the global temporal growth follow the same trend. The ellipsoid forebody is found spatially least stable while sharp cone is found to be most stable. However, the difference in the spatial growth rate reduces among all the three shapes in the streamwise direction towards the downstream. Thus, the effects of forebody shapes on the temporal and spatial stability of the boundary layer are similar (figure 6).

Figures 7a and 7b show spectra comparison for $N = 2$ and $N = 4$. It is found that increased azimuthal wave number reduces the difference in the temporal growth of eigenmodes for given forebody shapes.

Figure 6 presents the comparison of the velocity disturbance amplitudes (u, v and w) corresponding to the least stable eigenmodes. The least stable eigenmodes of all the three forebodies are having a frequency (ω_r)

almost equal to 0.15. The spatial growth of the disturbances is also found the largest for ellipsoid forebody and the least for the sharp cone. The order of magnitude for the w disturbances are almost four times higher than that of the u and v disturbances for all the three forebody shapes. A similar trend has been found that of temporal eigenmodes for the spatial eigenmodes of the sharp cone and paraboloid geometries. The magnitude of difference of u and v disturbances are too small in comparison to the w disturbances.
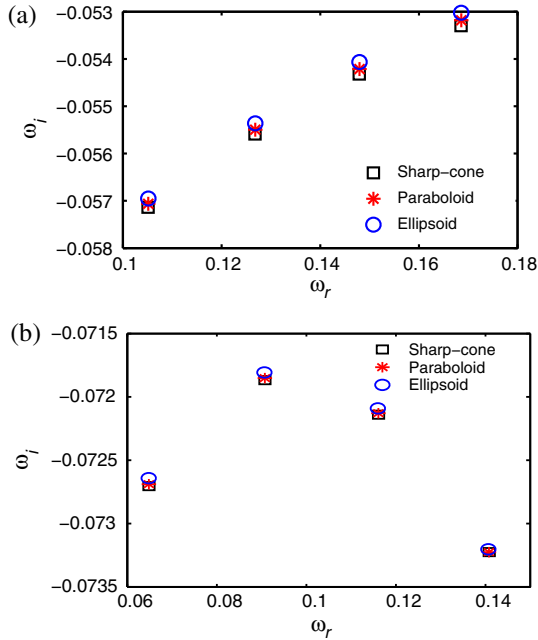
Figure 7. Spectra comparison for different forebody shapes at $Re = 2000$ and FR = 2.5. (**a**) $N = 2$, (**b**) $N = 4$.
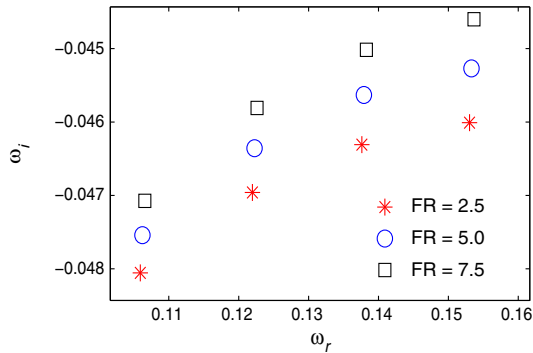

Figure 8. Comparison of the eigenspectra for different FR for the ellipsoid at $N = 1$ and $Re = 2000$.

4.4 *Effect of fineness ratio on temporal global modes*

The effect of fineness ratio on the temporal and spatial eigenmodes are discussed in this section. FR = 2.5, 5.0 and 7.5 are considered for $N = 1$ and $Re = 2000$. The size of the computational domain is the same for all the three forebody geometries. Figure 8 shows the comparison of the eigenspectra for ellipsoid forebody at $Re = 2000$ and $N = 1$ for different FR values. It is observed from figure 8 that the temporal growth (ω_i) is the highest for FR = 7.5 and the least for FR = 2.5. This indicates that increased FR increases the temporal growth rate.

To study the effect of FR on the spatial eigenmodes, the least stable eigenmodes are selected for each forebody with $\omega_r = 0.153$ and plotted at streamwise
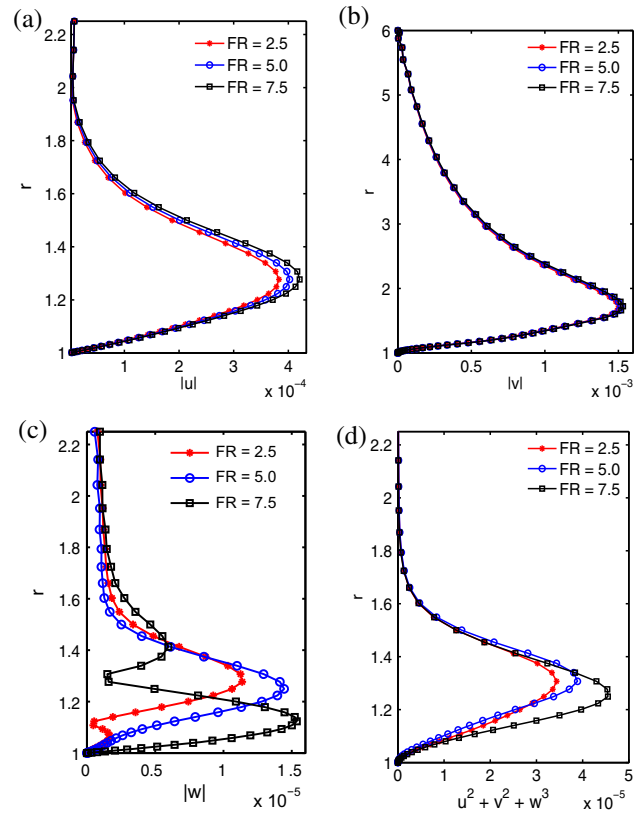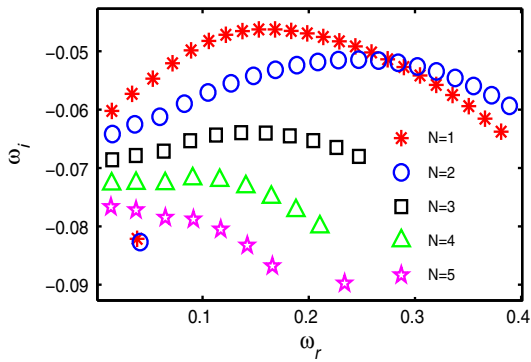

Figure 9. Comparison of the spatial eigenmodes at streamwise location $x = 75$ for the ellipsoid forebody at $N = 1$ and $Re = 2000$.

location $x = 75$. The disturbance amplitudes of u, v, and w, along with the total perturbation kinetic energy, have been compared for different FR values. The order of magnitude for the disturbance amplitude w is found very large in comparison to u and v. Similarly, for different values of FR, only marginal difference has been found in the magnitude of u and v while it is significant for w. The comparison of the disturbance kinetic energy for different FRs shows that the spatial growth of the disturbances is larger for FR = 7.5 and smaller for FR = 2.5. The temporal and spatial growth of disturbances were also studied for the paraboloid and sharp cone geometries, and similar results were found (figure 9).

4.5 *Effect of azimuthal wave number (N) on the temporal global modes*

In this section, we studied the effect of azimuthal wave numbers $N = 1, 2, 3, 4$ and 5 on the temporal and spatial growth of disturbances. The global modes are computed for $Re = 2000, 5000$ and 10000 for FR = 2.5, 5.0 and 7.5. Figure 10 shows the comparison of
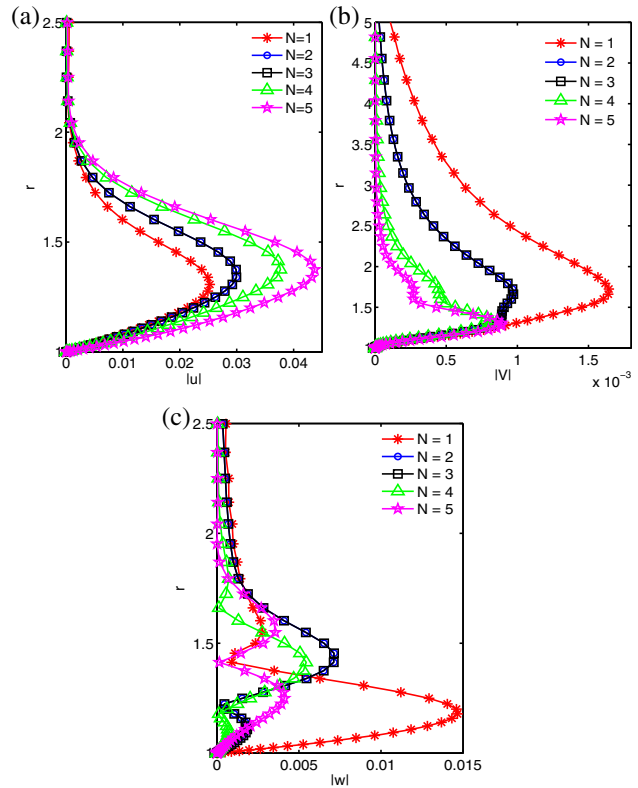
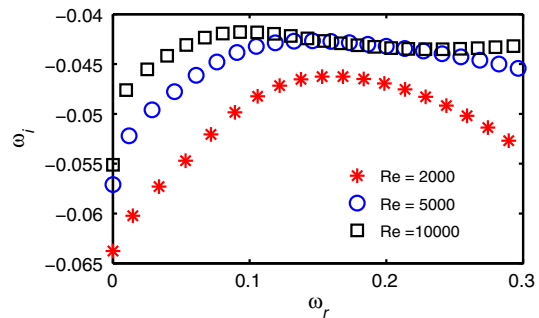**Figure 10.** Comparison of the eigenspectrum for the ellipsoid forebody for FR = 2.5 at $N = 1$ and $Re = 2000$.

eigenspectra for paraboloid forebody at $Re = 2000$ and FR = 2.5. It has been observed from figure 10 that the temporal growth (ω_i) is the highest for $N = 1$ and least for $N = 5$. Thus, the temporal growth reduces with the increased azimuthal wave number N. To compare the spatial growth rate of the disturbances, the eigenmodes with $\omega_r = 0.155$ have been selected for different azimuthal wave numbers. The spatial eigenmodes corresponding to these eigenmodes have been plotted at streamwise location $x = 75$, as shown in figure 11. It is found that increased azimuthal wave number has increased the spatial growth of u and w disturbances while reduced the spatial growth of v disturbances. The order of magnitude is found to be the highest for w disturbance amplitudes and lowest for v disturbances.

4.6 *Effect of Reynolds number (Re) on temporal global modes*

In this section, we studied the effect of Reynolds number $Re = 2000, 5000$ and 10000 on the temporal and spatial growth of disturbances. The global modes are computed for different forebody shapes and azimuthal wave numbers. Figure 12 shows the comparison of eigenspectra for three different Reynolds number for $N = 1$ and FR = 2.5. The temporal growth increases with the increase in Reynolds number. Figure 13 presents the comparison of the disturbance amplitudes near $\omega_r = 0.09$ and it is found that there is an increase in magnitudes of u and w disturbance amplitudes and a reduction in magnitude of v with an increase in Reynolds number. The overall disturbance kinetic energy within the boundary layer is higher for the higher Reynolds number. The boundary layer is found globally stable for the range of Reynolds number considered. The boundary layers are found convectively unstable. Generally, without absolute instability, there is no global instability. However,

Figure 11. Comparison of the spatial eigenmodes for $Re = 2000$, FR = 2.5, $\omega_r = 0.155$ and $x = 75$. (**a**) $|u|$, (**b**) $|v|$ and (**c**) $|w|$.


Figure 12. Comparison of the eigenspectrum for the paraboloid shape at $N = 1$ and FR = 2.5.

even with absolute instability, flow may be globally stable, at least flows which move slowly in the streamwise direction [27].

5. Conclusions

Global instability computations are performed on the axisymmetric boundary layer developed on a circular cylinder with different axisymmetric forebody shapes of FR = 2.5, 5.0 and 7.5. The forebody shapes of
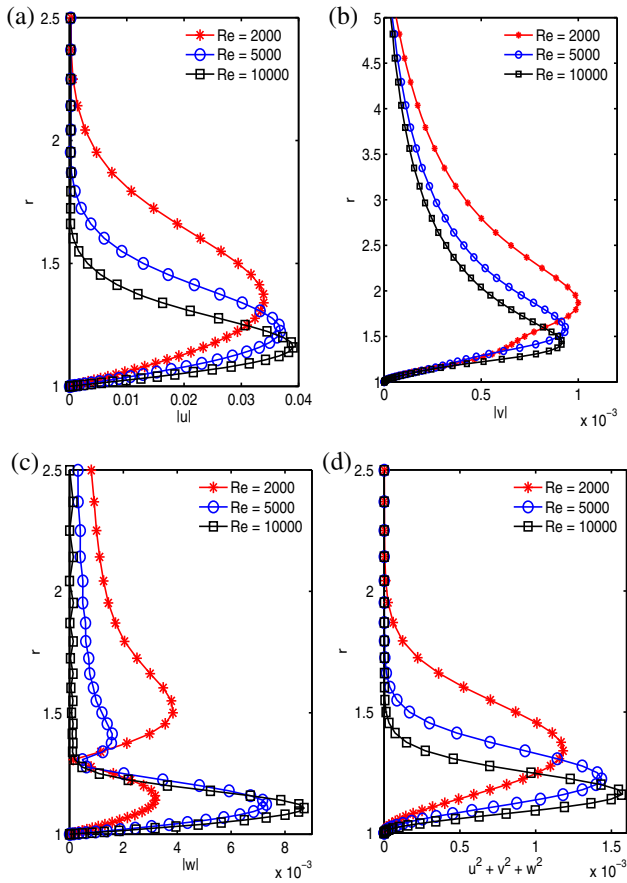
Figure 13. Comparison of the eigenfunctions for different forebody shapes at $N = 1$ and FR $= 2.5$.

paraboloid, ellipsoid and sharp cone have been considered for the stability analysis. The helical global modes with $N = 1, 2, 3, 4$ and 5 have been studied for $Re = 2000$, 5000 and 10000.

The temporal growth of helical modes for the ellipsoid forebody is found to be the least stable, and that of the sharp cone is found to be the most stable for given values of Re, N and FR. The difference in the temporal growth rate has been reduced between the global modes of different forebody shapes at higher Re. The spatial amplification of the disturbances is found more substantial in the azimuthal direction (w component) for given values of Re, N and FR. The difference in the spatial amplification is found marginal (very small) for different forebody shapes in the axial and radial directions, while it is found significant in the azimuthal direction. The order of disturbance amplitude magnitudes in the azimuthal direction is almost 4 to 5 times higher than that of the axial and radial directions. The temporal growth of the helical eigenmodes is found to be larger with larger value of FR at a given Re and N, irrespective of the shape of the forebody. However, it is not the case for axisymmetric global modes. The spatial growth of

the disturbances corresponding to the least stable eigenmodes is found larger for FR $= 7.5$ for all three forebody shapes. Similarly, the spatial growth of disturbances is found higher in the azimuthal direction for a given Re and N.

The global helical modes are found least stable for $N = 1$ and most stable for $N = 5$ for different forebody shapes at a given Re and FR. The temporal growth of $N = 1$ is found higher than $N = 2$ at lower frequency ($\omega_r < 0.28$) and lower at higher frequency ($\omega_r > 0.28$). The temporal growth is positive for helical modes $N = 1, 2$ and 3, upto some values of ω_r, and then it is negative. However, for helical modes, $N = 4$ and $N = 5$, the damping effect is found on the temporal growth with increased frequency. The gap between the two frequency values also increases with the increase in the azimuthal wave number (N). The spatial growth of disturbance amplitudes for the least stable eigenmodes is found highest in the radial and azimuthal directions for $N = 1$ and the least in the axial direction. The increase in Re increases the temporal growth of disturbances. The gap between the two discrete frequency values reduces with the increased Re. The spatial growth of the disturbance amplitudes is found larger at larger Re. The penetration of amplitudes is higher at lower Re due to strong viscous effects. Thus, the global modes of the boundary layer are found stable in the present study of the boundary layer.

References

[1] J S Parsons and R E Goodson, Technical report H, Automatic control center, School of Mechanical Engineering (Purdue University, 1972)
[2] V Narayanan and R Govindarajan, *Pramana – J. Phys.* **64(3)**, 323 (2005)
[3] M Casarella, T C Shen and B E Bowers, *Ship Aoustic Dept*. R & D Report **77** (1977)
[4] R L James, B H Navran and R A Rozenddal, NASA CR-166051 (1984)
[5] B J Holmes, C J Obara and L P Yip, NASA TP-2256 (1984)
[6] B H Carmichael, *Underwater missile propulsion* (Compass Publications, 1966)
[7] V Theofilis, *Prog. Aerosp. Sci*. **39**, 249 (2003)
[8] F Alizard and J C Robinet, P*hys. Fluid* **19**, 114105 (2007)
[9] E Akervik, U Ehrenstein, F Gallaire and D S Henningson, *Eur. J. Mech. B/Fluids* **27**, 501 (2008)
[10] G N V Rao, *J. Appl. Math. Phys*. **25**, 63 (1974)
[11] O R Tutty and W G Price, *Phys. Fluid* **14**, 628 (2002)
[12] R Bhoraniya and V Narayanan, *J. Phys.: Conf. Ser*. **822**, 012018 (2017)
[13] R Bhoraniya and V Narayanan, *Phys. Rev. Fluids* **2**, 063901 (2017)

[14] R Bhoraniya and V Narayanan, *Theor. Comput. Fluid Dyn.* **32**, 425 (2018)

[15] R Bhoraniya and V Narayanan, *Pramana – J. Phys.* **39(5)**, 93 (2019)

[16] U Ehrenstein and F Gallaire, *J. Fluid Mech.* **536**, 209 (2005)

[17] G Swaminathan, K Shau, A Sameen and R Govindarajan, *Theor. Compt. Fluid Dyn.* **25**, 53 (2011)

[18] R Bhoraniya and V Narayanan, *Fluid Dyn.* **54(5)**, 93 (2019)

[19] M Gaster, *J. Fluid Mech.* **22**, 433 (1965)

[20] A Michalke, *J. Fluid Mech.* **23**, 521 (1965)

[21] C K W Tam, *J. Fluid Mech.* **89**, 357 (1978)

[22] J M Chomaz, P Huerre and L G Redekopp, *Proc. Symp. Turbul. Shear flows*, 6th, Toulouse, Fr. **3.2**, 1 (1987)

[23] J M Chomaz, P Huerre and L G Redekopp, *Phys. Rev. Lett.* **60**, 25 (1988)

[24] R T Pierrehumbert, *J. Atmos. Sci.* **62**, 2141 (1984)

[25] W Koch, *J. Sound Vib.* **99**, 53 (1985)

[26] P A Monkewitz, D W Bechert, B Barsikow and B Lehmann, *J. Fluid Mech.* **31**, 999 (1988)

[27] P Huerre and P A Monkwwitz, *Annu. Rev. Fluid Mech.* **22**, 473 (1990)

[28] R S Lin and M R Malik, *J. Fluid Mech.* **311**, 239 (1996)

[29] R S Lin and M R Malik, *J. Fluid Mech.* **333**, 125 (1997)

[30] V Theofilis, P W Duck and J Owen, *J. Fluid Mech.* **505**, 249 (2004)

[31] V Theofilis, *Theor. Comput. Fluid Dyn.* **31**, 623 (2017)

[32] M R Malik, *J. Comput. Phys.* **86**(**2**), 372 (1990)